Spherical Wave Treatment of Laue Case Rocking Curves

U. Bonse and R. Teworte

Institut für Physik, Universität Dortmund

Dedicated to Professor G. Hildebrandt on the occasion of his 60th birthday

A spherical wave theory is given for the calculation of the observed fine structure of Laue case rocking curves [1—3] of a pair of perfect crystals.

It is shown that under the experimental condition of measuring simultaneously the full width of outgoing beams, the simple plane wave theory presented previously [1] yields identical results.

1. Introduction

Laue case rocking curves of a pair of perfect crystals (e.g. silicon) measured in $(n, -n)$ geometry have drawn renewed attention because of their oscillatory fine structure [1—3]. Provided that the product $\mu \cdot t$ of absorption coefficient μ and crystal thickness t is not too large ($\mu t \lesssim 1$) numerous oscillations over the whole range of the rocking curve can be resolved experimentally (Fig. 1) as long as high stability and noise protection of the experimental arrangement is guaranteed.
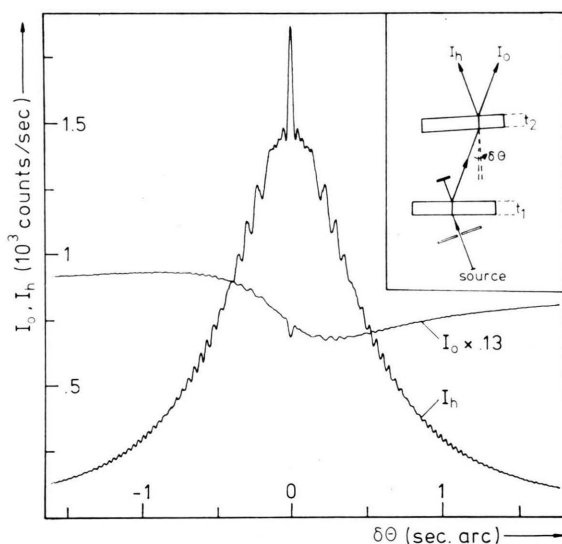

Fig. 1. Typical Laue-case rocking curve as obtained with the experimental arrangement shown in the inset. Si 511 reflection with Mo Ka$_1$ radiation, $t_1 = 692.5$ μm, $t_2 = 698.7$ μm.

Reprint requests to Prof. Dr. U. Bonse, Institut f. Physik, Universität Dortmund, Postfach 500500, 4600 Dortmund 50.

As has been pointed out in a previous paper [2] the nature of the oscillatory structure is extremely sensitive to $f_h t \lambda$, where f_h is the real part of the atomic scattering factor, λ the wavelength and t again the crystal thickness. Theoretical rocking curves calculated from a plane wave theory based upon the dynamical diffraction theory for perfect crystals are in excellent agreement with experiment. Hence from theoretical curves giving the best fit to the experimental ones the structure factor f_h can be determined with high precision. However, considering the experimental conditions described in reference [2] the question arises whether an incident-spherical-wave approximation would not be a more appropriate theoretical approach for calculating rocking curves. In order to solve this problem, we have performed the spherical-wave calculation which is presented below. As is finally shown, under the considered experimental conditions both the plane wave and the spherical-wave theory lead to the same result. Since the latter is more complicated we usually favour the plane-wave calculations in the evaluation of the experiments.

In the following we proceed by firstly calculating transmission factors for the amplitudes in plane-wave theory and obtain the spherical-wave solution by Fourier transformation.

2. Plane Wave Transmission Coefficients for Parallel-Sided Crystal Plates

For an incident plane wave (Figure 2)

$$\mathscr{D}_m^{\alpha i}(\boldsymbol{r}) = D_m^{\alpha i} \exp\left(2\pi i \, \boldsymbol{K}_m^i \, \boldsymbol{r}\right) \quad m = 0, h$$

with polarization state $\alpha = \sigma, \pi$ (for simplification α will be omitted in what follows) Bonse and Graeff [4] have derived amplitude ratios

Fig. 2. Definition of transmission factors, see text.

$$\langle m \mid 1,2 \mid n \rangle \equiv \frac{D_n^{\mathrm{p}}}{D_m^{\mathrm{i}}} \bigg|_{\text{via wavefields } 1,2} \quad m, n = 0, h$$

of the amplitudes of the incoming wave D_m^{i} and the outgoing wave D_n^{p} ("p" for plane wave) in the following form (Eqs. (4.19), (4.46), and (4.45), respectively, in Ref. 4): reflection "h":

$$\langle 0 \mid 1,2 \mid h \rangle = i \frac{C}{|C|} \left(\frac{\gamma_0}{\gamma_h}\right)^{1/2} \frac{\chi_h}{|(\chi_h \chi_{\bar{h}})^{1/2}|}$$
$$\cdot \exp[i a_h t + i(a_{rh} - a_{r0}) Z_f] \qquad (1)$$
$$\cdot \exp\left[i \frac{\pi}{\Delta_e}(t y + 2 Z_f y_r)\right] S(y, t)$$

reflection "$\bar{h}$":

$$\langle h \mid 1,2 \mid 0 \rangle = i \frac{C}{|C|} \left(\frac{\gamma_h}{\gamma_0}\right)^{1/2} \frac{\chi_{\bar{h}}}{|(\chi_h \chi_{\bar{h}})^{1/2}|}$$
$$\cdot \exp[i a_0 t - i(a_{rh} - a_{r0}) Z_f] \qquad (2)$$
$$\cdot \exp\left[-i \frac{\pi}{\Delta_e}(t y + 2 Z_f y_r)\right] S(y, t)$$

transmission "o":

$$\langle h \mid 1,2 \mid h \rangle = \exp(i a_h t) \exp\left(i \frac{\pi t}{\Delta_e} y\right)$$
$$\cdot [C(y, t) - i y S(y, t)] \qquad (3)$$

with abbreviations

$$\qquad\qquad\qquad\qquad\qquad\qquad\qquad (4)$$
$$S(y, t) \equiv \sin\left[\frac{\pi t}{\Delta_e}(y^2 + v^2)^{1/2}\right] / (y^2 + v^2)^{1/2},$$

$$C(y, t) \equiv \cos\left[\frac{\pi t}{\Delta_e}(y^2 + v^2)^{1/2}\right], \qquad (5)$$

$$v^2 \equiv \chi_h \chi_{\bar{h}} / |\chi_h \chi_{\bar{h}}|, \qquad (6)$$

$$\Delta_e \equiv (\gamma_0 \gamma_h)^{1/2} / [k \mid C (\chi_h \chi_{\bar{h}})^{1/2} \mid], \qquad (7)$$

$$y = - k \Delta\theta \cdot \Delta_e \sin 2\theta_B / \gamma_h$$
$$\qquad - k \chi_0 \Delta_e (\gamma_h^{-1} - \gamma_0^{-1})/2, \qquad (8)$$

$$\gamma_m = \boldsymbol{z} \cdot \boldsymbol{K}_m / |\boldsymbol{K}_m|, \quad m = 0, h, \qquad (9)$$

$$a_m = \pi k \chi_0 / \gamma_m, \qquad (10)$$

$$C = \begin{cases} 1, & \sigma\text{-polarization}, \\ \cos 2\theta_B, & \pi\text{-polarization}, \end{cases} \qquad (11)$$

$$k = \lambda^{-1}; \qquad (12)$$

t is the crystal thickness, λ the wavelength. $\boldsymbol{z}$ is the normal pointing into the crystal at the entrance surface.

The origin of the coordinate system lies in the source with the entrance surface having a distance $Z_f = \boldsymbol{r} \cdot \boldsymbol{z}$ from the source (Figure 2). $\Delta\theta \equiv \theta - \theta_B$ measures the deviation of the incoming beam from the kinematical Bragg angle θ_B. Subscripts r, i denote real and imaginary parts of complex quantities, respectively. Note that absorption is included by complex values of the dielectric susceptibility χ. By

$$\mu_0 = 2 \pi k \chi_{i0} \qquad (13)$$

the normal absorption coefficient μ_0 is related to
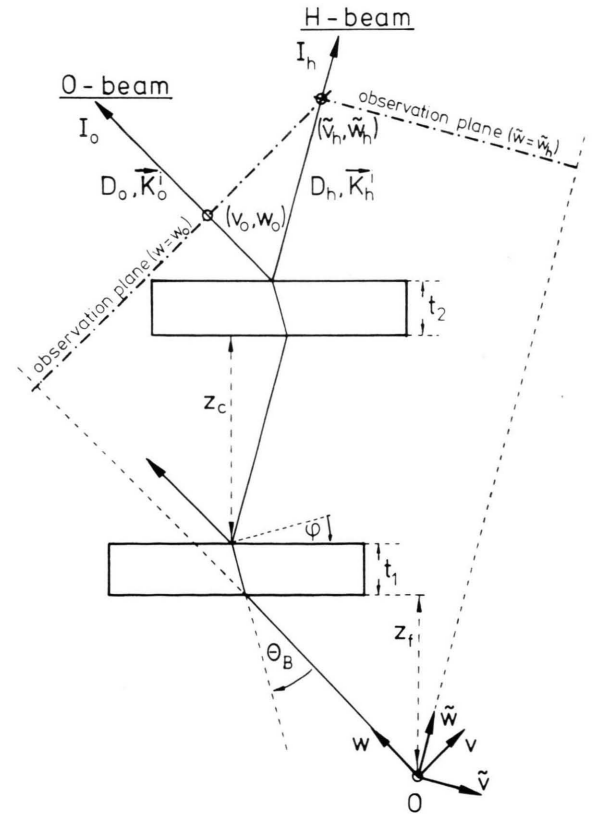
Fig. 3. Diffraction by two crystal plates and definition of the coordinate systems $\boldsymbol{u}$, $\boldsymbol{v}$, $\boldsymbol{w}$ and $\boldsymbol{u}$, $\tilde{\boldsymbol{v}}$, $\tilde{\boldsymbol{w}}$; $\boldsymbol{u}$ is oriented normal to the plane of the figure.

χ_{10} which is the imaginary part of χ averaged over the unit cell.

We now apply formulas (1) through (3) and (13) to the ray geometry shown in Fig. 3 in which diffraction by two crystal plates of identical crystallographic orientation is considered. We derive for the amplitudes D_0^p and D_h^p of the plane waves of beams O and H behind the second crystal plate as function of y (effectively determined by the angle of incidence of the incoming plane wave) and of δy, (effectively determined by the deviation of parallel orientation):

O-beam:

$$D_0^p(y, \delta y) = \langle 0 | 1, 2 | h \rangle \Big|_{\substack{y \to y \\ Z_t \to Z_t \\ t \to t_1}} \langle h | 1, 2 | 0 \rangle \Big|_{\substack{y \to y + \delta y \\ Z_t \to Z_t + t_1 + Z_c \\ t \to t_2}} \cdot D_0^i$$

$$= v^2 \exp\left[-\frac{\mu_0 T}{4}(\gamma_0^{-1} + \gamma_h^{-1})\right] \exp\left[i \Phi_0(t_1, t_2, Z_f, Z_c)\right] \exp\left[-\frac{i\pi}{\Delta_e}(T + 2Z_c) y_r\right]$$

$$\cdot S(y, t_1) S(y + \delta y, t_2) D_0^i; \tag{14}$$

H-beam:

$$D_h^p(y, \delta y) = \langle 0 | 1, 2 | h \rangle \Big|_{\substack{y \to y \\ Z_t \to Z_t \\ t \to t_1}} \langle h | 1, 2 | h \rangle \Big|_{\substack{y \to y + \delta y \\ Z_t \to Z_t + t_1 + Z_c \\ t \to t_2}} \cdot D_0^i$$

$$= \frac{C}{|C|} \left(\frac{\gamma_0}{\gamma_h}\right)^{1/2} \frac{\chi_h}{|(\chi_h \chi_{\bar{h}})^{1/2}|} \exp\left[-\frac{\mu_0 T}{4}(\gamma_0^{-1} + \gamma_h^{-1})\right] \exp\left[i \Phi_h(t_1, t_2, Z_f)\right]$$

$$\cdot \exp\left[i \frac{\pi}{\Delta_e}(T + 2Z_f) y_r\right] S(y, t_1) [C(y + \delta y, t_2) - i(y + \delta y) S(y + \delta y, t_2)] D_0^i. \tag{15}$$

The crystals are a distance Z_c apart. t_1, t_2 are their respective thicknesses. Furthermore, we have introduced the total thickness

$$T \equiv t_1 + t_2 \tag{16}$$

and the phases

$$\Phi_0(t_1, t_2, Z_f, Z_c) \equiv a_{r0} T - (a_{rh} - a_{r0}) Z_c$$
$$- \frac{\pi}{\Delta_e}(2Z_f + 2Z_c + t_1 + T) \delta y + \pi, \tag{17}$$

$$\Phi_h(t_1, t_2, Z_f) \equiv a_{rh} T + (a_{rh} - a_{r0}) Z_f$$
$$+ \frac{\pi}{\Delta_e} t_2 \delta y + \pi/2. \tag{18}$$

The wave vectors are

$$\boldsymbol{K}_0^i(y) = \boldsymbol{K}_{0B} + \Delta \boldsymbol{K}_0^i(y) \tag{19}$$

for the O-beam and

$$\boldsymbol{K}_h^i(y) = \boldsymbol{K}_{0B} + \boldsymbol{h} + \Delta \boldsymbol{K}_h^i(y) \tag{20}$$

for the H-beam (Figure 3). $\boldsymbol{K}_{0B}$ corresponds to incidence at the exact Bragg angle θ_B. $\boldsymbol{h}$ is the reciprocal lattice vector.

With the help of Fig. 4 we derive

$$|\Delta \boldsymbol{K}_h^i(y)| = \gamma_h/\gamma_0 |\Delta \boldsymbol{K}_h^i(y)|. \tag{21}$$

Since $\Delta \boldsymbol{K}_h^i(y)$ and $\Delta \boldsymbol{K}_0^i(y)$ differ by $2\theta_B$ in direction we have

$$\tag{22}$$

$$\frac{\Delta \boldsymbol{K}_h^i(y)}{|\Delta \boldsymbol{K}_h^i(y)|} = \begin{pmatrix} \cos 2\theta_B, & \sin 2\theta_B \\ -\sin 2\theta_B, & \cos 2\theta_B \end{pmatrix} \frac{\Delta \boldsymbol{K}_0^i(y)}{|\Delta \boldsymbol{K}_0^i(y)|}.$$
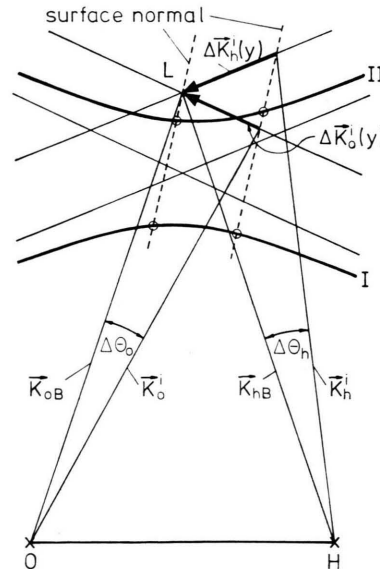

Fig. 4. Dispersion surface.

Combining (21) and (22) we find

$$\Delta \boldsymbol{K}_h^{\text{i}}(y) = \frac{\gamma_h}{\gamma_0} \begin{pmatrix} \cos 2\theta_{\text{B}}, & \sin 2\theta_{\text{B}} \\ -\sin 2\theta_{\text{B}}, & \cos 2\theta_{\text{B}} \end{pmatrix} \Delta \boldsymbol{K}_0^{\text{i}}(y). \quad (23)$$

3. Spherical-wave Diffraction

In the spherical-wave approximation first investigated by Kato [5] the whole dispersion surface is uniformly and coherently excited which, together with a narrow incident beam, leads to a spacial intensity distribution. This is in contrast to the plane wave case where an angular intensity distribution is obtained together with (in principle) an infinitely wide and homogeneous beam.

A suitable way of calculating the special intensity distributions $I_0^{\text{s}}(v, \delta y)$ and $I_h^{\text{s}}(\tilde{v}, \delta y)$ of spherical waves behind two crystals diffracting in the Laue case (v, $\tilde{v}$ are coordinates normal to the outgoing beams) is to represent the incident spherical wave as an infinite set of coherent plane-waves with proper phases, i.e. as the Fourier expansion

$$\frac{\exp(2\pi i k r)}{r} = \frac{1}{\pi} \int \text{d}^3 k \quad (24)$$
$$\cdot \exp(2\pi i \boldsymbol{K} r)(\boldsymbol{K}^2 - k^2)^{-1}.$$

$\boldsymbol{K}$ is defined with respect to the coordinate system $\boldsymbol{u}$, $\boldsymbol{v}$, $\boldsymbol{w}$ or $\boldsymbol{u}$, $\tilde{\boldsymbol{v}}$, $\tilde{\boldsymbol{w}}$, respectively (Fig. 3) as

$$\boldsymbol{K} = (K_u, K_v, K_w) \quad (25)$$

or

$$\boldsymbol{K} = (K_u, K_{\tilde{v}}, K_{\tilde{w}}). \quad (26)$$

In the u, v, w-system

$$\boldsymbol{K}_{0\text{B}} = k(0, 0, 1). \quad (27)$$

Correspondingly in the u, $\tilde{v}$, $\tilde{w}$-system:

$$\boldsymbol{K}_{0\text{B}} + \boldsymbol{h} = k(0, 0, 1). \quad (28)$$

On passing the crystals, each plane wave undergoes amplitude and phase modulation according to (14) and (15). We carry out integration with respect to K_w ($K_{\tilde{w}}$) and K_u in the plane $u = 0$, which is defined by the reciprocal lattice vector $\boldsymbol{h}$ and $\boldsymbol{K}_{0\text{B}}$. Together with (19, 20) and (23) we find the result [6—7]:

$$\mathscr{D}_m^{\text{s}}(\delta y) = (kw)^{-1/2} \exp\left\{ i\pi/4 + 2\pi i [\boldsymbol{K}_{0\text{B}} + \boldsymbol{h}\,\delta_{hm}] \cdot \boldsymbol{r} \right\}$$
$$\cdot \int\limits_{-\infty}^{+\infty} \text{d}K_{lvm} D_m^{\text{p}}(y, \delta y) \exp(2\pi i \Delta \boldsymbol{K}_m^{\text{i}}(y) \cdot \boldsymbol{r}), \quad m = 0, h, \quad \begin{array}{l} l = v \text{ if } m = 0, \\ = \tilde{v} \text{ if } m = h. \end{array} \quad (29)$$

Here the integration over $\text{d}K_{vm}$, $\text{d}K_{\tilde{v}m}$ is in fact one with respect to the variable $\Delta\theta$ (or, equivalently, y, the deviation from the exact Bragg angle). δ_{hm} is the Kronecker symbol. $\boldsymbol{K}_0^{\text{i}}$ of (19) is restricted by

$$\boldsymbol{K}_0^{\text{i}} = (\text{O}, K_v, (k^2 - K_v^2)^{1/2}. \quad \text{We set} \quad K_v = -k\Delta\theta. \quad (30), (31)$$

Expanding $\Delta\boldsymbol{K}_0^{\text{i}}(y)$ and $\Delta\boldsymbol{K}_h^{\text{i}}(y)$ to second order in $\Delta\theta$ and introducing the parameter y by using (8), we obtain

$$\mathscr{D}_0^{\text{s}}(\delta y) = \frac{Hv^2}{(kw)^{1/2}} \exp\left\{ -\frac{\mu_0 T}{4}(\gamma_0^{-1} + \gamma_h^{-1}) \right\}$$
$$\cdot \exp\left\{ i\pi \left[\frac{1}{4} + 2HLv + \left(2k - \frac{H^2 L^2}{k} \right) w \right] + i\Phi_0(t_1, t_2, Z_{\text{f}}, Z_{\text{c}}) \right\} E_0 D_0^{\text{i}}, \quad (32)$$

$$E_0 \equiv \int\limits_{-\infty}^{+\infty} \text{d}y_{\text{r}} \exp\left\{ 2\pi i \left[\left(-\frac{T + 2Z_{\text{c}}}{2\Delta_{\text{e}}} - \frac{H^2}{k} w + Hv \right) y_{\text{r}} - \frac{H^2}{2k} w y_{\text{r}}^2 \right] \right\} S(y, t_1) S(y + \delta y, t_2), \quad (33)$$

and furthermore

$$\mathscr{D}_h^{\text{s}}(\delta y) = \frac{HC}{(k\tilde{w})^{1/2}|C|} \left(\frac{\gamma_h}{\gamma_0} \right)^{1/2} \frac{\chi_h}{|(\chi_h \chi_{\bar{h}})^{1/2}|} \exp\left[-\frac{\mu_0 T}{4}(\gamma_0^{-1} + \gamma_h^{-1}) \right]$$
$$\cdot \exp\left\{ i\pi \left[\frac{1}{4} + 2\frac{\gamma_h}{\gamma_0} HL\tilde{v} + \left(2k - \frac{\gamma_h}{\gamma_0}\frac{H^2 L^2}{k} \right) \tilde{w} \right] + i\Phi_h(t_1, t_2, Z_{\text{f}}) \right\} E_h D_0^{\text{i}}, \quad (34)$$

$$E_h \equiv \int\limits_{-\infty}^{+\infty} \text{d}y_{\text{r}} \exp\left\{ 2\pi i \left[\left(\frac{T + 2Z_{\text{f}}}{2\Delta_{\text{e}}} - \frac{\gamma_h}{\gamma_0}\frac{H^2}{k} \tilde{w} + \frac{\gamma_h}{\gamma_0} H\tilde{v} \right) y_{\text{r}} - \frac{\gamma_h}{\gamma_0}\frac{H^2}{2k} \tilde{w} y_{\text{r}}^2 \right] \right\}$$
$$\cdot S(y, t_1)[C(y + \delta y, t_2) - i(y + \delta y) S(y + \delta y, t_2)] \quad (35)$$

with

$$H \equiv \gamma_h (\Delta_e \sin 2\theta_B)^{-1}, \tag{36}$$

$$L \equiv \frac{\Delta_e}{2\pi} a_{r0} \left(\frac{\gamma_0}{\gamma_h} - 1 \right). \tag{37}$$

From the amplitudes of (32) and (34) we calculate the intensities $I_0^s(v, \delta y)$ and $I_h^s(\tilde{v}, \delta y)$ measured in observation planes $w = w_0$ and $\tilde{w} = \tilde{w}_h$ normal to beam O and beam H, respectively (Figure 3).

From (32) we calculate

$$I_0^s(v, \delta y) \equiv \mathscr{D}_0^s(\delta y) \cdot \mathscr{D}_0^{s*}(\delta y) = \frac{H^2 |v^2|^2}{k w_0} \exp \left\{ -\frac{\mu_0 T}{2} (\gamma_0^{-1} + \gamma_h^{-1}) \right\}$$
$$\cdot \int_{-\infty}^{+\infty} \int_{-\infty}^{+\infty} dy_r \, dy_r' \exp \left\{ 2\pi i \left[\left(-\frac{T + 2Z_c}{2\Delta_e} - \frac{H^2}{k} w_0 + Hv \right) (y_r - y_r') - \frac{H^2}{2k} w_0 (y_r^2 - y_r'^2) \right] \right\}$$
$$\cdot S(y, t_1) S^*(y', t_1) S(y + \delta y, t_2) S^*(y' + \delta y, t_2) |D_0^i|^2. \tag{38}$$

In the experiment 1—3 the detector measures simultaneously the total beam. We therefore have to integrate over the coordinate v:

$$I_0^s(\delta y) \equiv \int_{-\infty}^{+\infty} dv \, I_0^s(v, \delta y). \tag{39}$$

Since v occurs only in the term $Hv(y_r - y_r')$ in the exponent of (38), the integration involves

$$\int_{-\infty}^{+\infty} dv \exp \{2\pi i Hv(y_r - y_r')\} = H^{-1} \delta(y_r - y_r'). \tag{40}$$

With (40) we calculate

$$I_0^s(\delta y) = \frac{H|v^2|^2}{k w_0} \exp \left\{ -\frac{\mu_0 T}{2} (\gamma_0^{-1} + \gamma_h^{-1}) \right\} \int_{-\infty}^{+\infty} dy \, |S(y, t_1)|^2 |S(y + \delta y, t_2)|^2 |D_0^i|^2. \tag{41}$$

In a totally analogous way we obtain from (34) for the H-beam:

$$I_h^s(\delta y) = \frac{H}{k \tilde{w}_h} \left| \frac{\chi_h}{\chi_{\bar{h}}} \right| \frac{\gamma_h}{\gamma_0} \exp \left\{ -\frac{\mu_0 T}{2} (\gamma_0^{-1} + \gamma_h^{-1})^{-1} \right\}$$
$$\cdot \int_{-\infty}^{+\infty} dy \, |S(y, t_1)|^2 |C(y + \delta y, t_2) - i(y + \delta y) S(y + \delta y, t_2)|^2 |D_0^i|^2. \tag{42}$$

Equations (41) and (42) are in effect the solutions obtained previously with the plane wave treat-

ment! The equivalence of either modes of treatment under the experimental conditions described above has thus been shown. An essential point for this to be true is obviously that the detector integrates over real space. What has been proved above is a special case of the more general Parseval-Theorem [8] stating that integrations in reciprocal space and in real space yield identical intensities.

In practise, (41) and (42) are fairly easily evaluated by convoluting the plane-wave case intensities, i.e. the plane-wave intrinsic reflection- and transmission curves of the two crystal plates.

An example of how good an agreement between theory and experiment is achievable is given below (Figure 5).
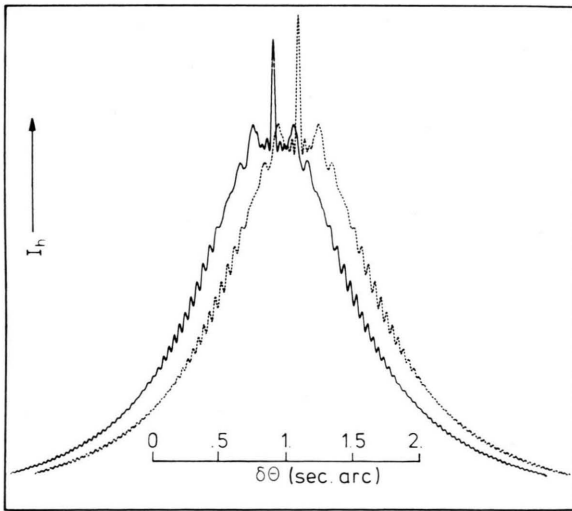
Fig. 5. Comparison of experimental (———) and theoretical (-----) rocking curves in the case of silicon 422 reflection, Ag Kα1 radiation. Curves have been shifted horizontally with respect to each other.

[1] U. Bonse, W. Graeff, R. Teworte, and H. Rauch, phys. stat. sol. (a) **43**, 487 (1977).
[2] U. Bonse and R. Teworte, J. Appl. Cryst. **13**, 410 (1980).
[3] R. Teworte and U. Bonse, Acta Cryst. **A 37**, C-270 (1981).
[4] U. Bonse and W. Graeff, in: X-Ray Optics, Ed. H.-J. Queisser, Springer-Verlag, Berlin 1977.
[5] N. Kato, Z. Naturforsch. **15 a**, 369 (1960).
[6] N. Kato, J. Appl. Phys. **39**, 2225 (1968).
[7] W. Bauspiess, U. Bonse, and W. Graeff, J. Appl. Cryst. **9**, 68 (1976).
[8] S. Kaczmarz and H. Steinhaws, in: Theorie der Orthogonalreihen, Chelsea Publishing Company, New York 1951.